Generation of tumorigenic porcine pancreatic ductal epithelial cells: toward a large animal model of pancreatic cancer

Neeley Remmers[1,2], Jesse L. Cox[3], James A. Grunkemeyer[4], Shruthi Aravind[1,2], Christopher K. Arkfeld[1,2], Michael A. Hollingsworth[4], Mark A. Carlson[1,2,5*]

[1]Department of Surgery, University of Nebraska Medical Center, Omaha, NE, USA

[2] Surgery Department, VA Nebraska-Western Iowa Health Care System, Omaha, NE, USA

[3]Department of Pathology and Microbiology, University of Nebraska Medical Center, Omaha, NE, USA

[4]Eppley Cancer Institute, University of Nebraska Medical Center, Omaha, NE, USA

[5]Department of Genetics, Cell Biology and Anatomy, University of Nebraska Medical Center, Omaha, NE, USA

*Corresponding author

Email: macarlso@unmc.edu (MAC)

Abstract

Background. A large animal model of pancreatic cancer would permit development of diagnostic and interventional technologies not possible in murine models, and also would provide a more biologically-relevant platform for penultimate testing of novel therapies, prior to human testing. Here, we describe our initial studies in the development of an autochthonous, genetically-defined, large animal model of pancreatic cancer, using immunocompetent pigs.

Methods. Primary pancreatic epithelial cells were isolated from pancreatic duct of domestic pigs; epithelial origin was confirmed with immunohistochemistry. Three transformed cell lines subsequently were generated from these primary cells using expression of oncogenic KRAS and dominant negative p53, with/without knockdown of p16 and SMAD4. We tested these cell lines using *in vitro* and *in vivo* assays of transformation and tumorigenesis.

Results. The transformed cell lines outperformed the primary cells in terms proliferation, population doubling time, soft agar growth, 2D migration, and Matrigel invasion, with the greatest differences observed when all four genes (KRAS, p53, p16, and SMAD4) were targeted. All three transformed cell lines grew tumors when injected subcutaneously in nude mice, demonstrating undifferentiated morphology, mild desmoplasia, and staining for both epithelial and mesenchymal markers. Injection into the pancreas of nude mice resulted in distant metastases, particularly when all four genes were targeted.

Conclusions. Tumorigenic porcine pancreatic cell lines were generated. Inclusion of four genetic "hits" (KRAS, p53, p16, and SMAD4) appeared to produce the best results in our *in vitro* and *in vivo* assays. The next step will be to perform autologous or syngeneic implantation of these cell lines into the pancreas of immunocompetent pigs. We believe that the resultant large animal model of pancreatic cancer could supplement existing murine models, thus improving preclinical research on diagnostic, interventional, and therapeutic technologies.

Introduction

In the United States in 2016, approximately 53,000 people (48% female) were diagnosed with pancreatic cancer (~3.1% of all new cancer diagnoses), and there were ~42,000 deaths (49% female) from pancreatic cancer (~7.0% of all cancer deaths) [*1,2*]. The lifetime risk for pancreatic cancer is approximately 1 in 65 [*1,2*]. The incidence of pancreatic cancer has been gradually increasing since the mid-1990's, and generally is higher in the African-American population [*1,2*]. Pancreatic cancer is now is the fourth most common cause of cancer-related death in both men and women (after lung, prostate, and colorectal cancer, or lung, breast, and colorectal cancer, respectively) [*1,2*]. Despite apparent advances in treatment modalities and strategies [*3*], mortality from pancreatic cancer has not decreased [*1,2*]. As of 2012, the U.S. overall 5-year survival rate from pancreatic cancer was 7.7%; 5-year survival rates in localized, regional (nodal spread), or metastatic disease were 29.3, 11.1, and 2.6%, respectively [*1,2*]. So there remains a need for improved early diagnosis and therapy for pancreatic cancer.

Rodent models of pancreatic cancer may not accurately reflect human biology because of differences in physiology, anatomy, immune response, and genetic sequence between the two species [*4-7*]. Remarkably, only 5-8% of anti-cancer drugs that emerged from preclinical studies and entered clinical studies have been ultimately approved for clinical use [*8,9*]. The cause of this low approval rate is multifactorial, but likely includes the less-than-optimal predictive ability of some murine models (e.g., tumor xenografting into immunosuppressed mice) to determine the efficacy of various therapeutics in humans [*4-6,10-14*]. Moreover, there are a number of genes for which the genotype-phenotype relationship is discordant between mice and human, including $CFTR^{-/-}$ and $APC^{+/-}$ [*15,16*]. Incidentally, both the porcine $CFTR^{-/-}$ and $APC^{+/-}$ mutants reiterate

74 the human phenotype (pulmonary/GI disease and rectal polyposis, respectively) [*15-17*], in
75 contradistinction to the murine mutants.
76 In fairness, the recent trend to employ genetically-engineered mouse models (GEMM),
77 patient-derived xenografts (PDX), humanized mice, and *in vivo* site-directed CRISPR/Cas9
78 gene-edited mice in the testing of anti-cancer therapeutics may yield murine models with better
79 predictive ability than obtained with previously [*6,18-22*]. Though promising, these more
80 advanced murine models come with increased cost and complexity [*20*], and experience with
81 them still is early. Importantly, all murine models have limited utility in the development of
82 diagnostic or interventional technology that requires an animal subject whose size approximates
83 a human. So at present, there remains a need for improved animal models of pancreatic cancer
84 that (1) are more predictive of human response to anti-cancer therapy [*20,22*], and (2) are of
85 adequate size for development of specific technologies. Herein we describe some initial steps
86 taken in the development of a genetically-defined, autochthonous model of pancreatic cancer in
87 immunocompetent pigs.
88

Materials and Methods

Standards, rigor, reproducibility, and transparency

The animal studies of this report were designed, performed, and reported in accordance with both the ARRIVE recommendations (Animal Research: Reporting of *In Vivo* Experiments [*23*]) and the National Institutes of Health Principles and Guidelines for Reporting Preclinical Research [*24,25*]; for details, refer to Tables S1 and S2, respectively.

Materials and animal subjects

All reagents were purchased through Thermo Fisher Scientific (www.thermofisher.com) unless otherwise noted. Short DNA sequences for vector construction, mutagenesis, and amplification purposes are shown in Table S3. Antibody information is given in Table S4. Wild type domestic swine (male and female; age 3 months at time of purchase; 30-32 kg) were purchased from the Animal Research and Development Center of the University of Nebraska Lincoln (ardc.unl.edu). Athymic homozygous nude mice (Crl:NU(NCr)-*Foxn1*^{nu}; female; 8-9 weeks old) were purchased from Charles River Laboratories, Inc. (www.criver.com). Primers utilized in this report (Table S3) were synthesized by Integrated DNA Technologies, Inc. (www.idtdna.com). DNA sequencing was performed by the UNMC Genomics Core Facility (www.unmc.edu/vcr/cores/vcr-cores/genomics). Oncopigs [*26*] were purchased from the National Swine Resource and Research Center (NSRRC; www.nsrrc.missouri.edu).

Animal welfare

The animals utilized to generate data for this report were maintained and treated in accordance with the *Guide for the Care and Use of Laboratory Animals* (8th ed.) from the National Research Council and the National Institutes of Health [*27*], and also in accordance with the Animal Welfare Act of the United States (U.S. Code 7, Sections 2131 – 2159). The animal protocols pertaining to this manuscript were approved by the Institutional Animal Care and Use Committee (IACUC) of the VA Nebraska-Western Iowa Health Care System (ID numbers 00927, 00937, 00998, and 01017) or by the IACUC of the University of Nebraska Medical Center (ID number 16-133-11-FC). All procedures were performed in animal facilities approved by the Association for Assessment and Accreditation of Laboratory Animal Care International (AAALAC; www.aaalac.org) and by the Office of Laboratory Animal Welfare of the Public Health Service (grants.nih.gov/grants/olaw/olaw.htm). All surgical procedures were performed under isoflurane anesthesia, and all efforts were made to minimize suffering. Euthanasia was performed in accordance with the AVMA Guidelines for the Euthanasia of Animals [*28*].

Porcine operative procedures

Further details on transgenic porcine subjects and related welfare, safety, husbandry, operative procedures, and perioperative management are given in the Supporting Information.

Isolation of porcine pancreatic ductal epithelial cells

A detailed protocol for isolation of porcine pancreatic ductal epithelial cells is provided in the Supporting Information (**Protocol S1**). In brief, the intact pancreas from male porcine research subjects (age 5 mo) was harvested within 5 min after euthanasia, which was

134 accomplished by transection of the intrathoracic inferior vena cava and exsanguination while
135 under deep isoflurane anesthesia. These pigs had been on a protocol to study biomaterials within
136 skin wounds of the dorsum. The subject had not received any recent medication other the
137 anesthetics given for euthanasia; buprenorphine and cefovecin sodium had been given 4 weeks
138 prior to euthanasia. Immediately after explantation of the pancreas, the main pancreatic duct was
139 dissected sterilely with micro instruments from the organ body under 3.5x loupe magnification.
140 The duct then was mechanically digested by passage through a 70 µm sieve (Corning™ Sterile
141 Cell Strainers, Thermo Fisher Scientific, cat. no. 07-201-431).
142 The collected fragments were enzymatically digested with 1 mg/mL of Collagenase D at
143 37˚C for 1 h with gentle shaking. The cells were pelleted (600 *g* x 5 min), the supernatant was
144 discarded, the cell pellet was resuspended in whole media, which was defined as: DMEM (high
145 glucose with L-glutamine; Thermo Fisher Scientific, cat. no. 12100-046) supplemented with
146 10% (final concentration) fetal bovine serum (FBS; Thermo Fisher Scientific, cat. no. 26140079)
147 and 1% Antibiotic-Antimycotic Solution (Corning Inc., cat. no. 30-004-CI; cellgro.com). Cell
148 concentration in the resuspension was determined with a hemocytometer, and cells then were
149 diluted and pipetted into a 96-well plate (1-10 cell/well, 100-200 µL/well). After 5-7 days of
150 culture under standard conditions (whole media, 37˚C, 5% CO_2), wells that contained cells with
151 epithelial-like morphology were trypsinized and re-plated into a new 96-well plate, in order to
152 dilute out any fibroblasts. Cells were passaged in this fashion at least four times, until no cells
153 with fibroblast morphology were present. The resulting cells were passaged up to a T25 flask,
154 and maintained with standard conditions.
155

156 # Generation of p53 and KRAS mutants and construction of
157 # expression vector

158 In order to generate the porcine $p53^{R167H}$ mutant, wild-type p53 cDNA first was amplified
159 from cervical lymph node tissue, which was obtained <5 min after euthanasia of a 4-month-old
160 male domestic swine that had been on an unrelated research protocol. In brief, fresh nodal tissue
161 was flash-frozen in liquid N_2 and then pulverized with a mortar and pestle, with continual
162 addition of liquid N_2 during pulverization. The frozen powder then was placed into the first
163 buffer solution of the QIAGEN RNEasy Mini Kit (cat. no. 74104; www.qiagen.com), and total
164 RNA was isolated per the manufacturer's instructions.

165 After isolation, the total RNA underwent reverse transcription to cDNA with a Verso
166 cDNA Synthesis Kit (Thermo Fisher Scientific, cat. no. AB1453A), per the manufacturer's
167 instructions. The wild type p53 sequence was amplified out of the cDNA using the PCR primers
168 shown in Table S3, which flanked the p53 cDNA with *Sal*I and *Bam*HI restriction sites.
169 Successful amplification of the wild-type p53 cDNA was confirmed by inserting the amplified
170 candidate sequence into the TOPO® vector (TOPO® TA Cloning® Kit; Invitrogen™/Life
171 Technologies™, Thermo Fisher Scientific, cat. no. K202020) per the manufacturer's
172 instructions, followed by sequencing.

173 Site-directed mutation of wild-type p53 into $p53^{R167H}$ was performed using Agilent
174 Technologies' QuickChange II Site-Directed Mutagenesis Kit (cat. no. 200523;
175 www.genomics.agilent.com) with the mutagenic primers shown in Table S3, per the
176 manufacturer's instructions. Presence of the $p53^{R167H}$ mutation was verified by sequencing as
177 described above. The multiple cloning site of a pIRES2-AcGFP1 Vector (Takara Bio USA, Inc.,

178 cat. no. 632435; www.clontech.com; manufacturer's vector information included as **Fig. S1**) was
179 cut with *Sal*I and *Bam*HI, and the p53^{R167H} sequence then was ligated into this plasmid.
180 The source of the porcine KRAS^{G12D} mutant was the plasmid used to generate the
181 p53/KRAS Oncopig [*26,29*]. The KRAS^{G12D} cDNA was amplified out of this plasmid with
182 primers (see Table S3) that flanked the sequence with *Xho*I and *Pst*I restriction sites. The
183 amplified product was inserted into the TOPO vector and verified by sequencing, as described
184 above. The above pIRES2-AcGFP1 Vector (already containing the p53^{R167H} sequence) then was
185 cut with *Xho*I and *Pst*I, and the KRAS^{G12D} sequence was ligated into this plasmid, producing a
186 pIRES2-AcGFP1 Vector which contained both mutant cDNAs within its multiple cloning site
187 (KRAS^{G12D} upstream).
188 The newly-constructed plasmid, hereafter designated as GKP (G = AcGFP1; K =
189 KRAS^{G12D}; P = p53^{R167H}), was transformed into One Shot™ Stbl3™ Chemically Competent *E.*
190 *coli* (Invitrogen™/Thermo Fisher Scientific, cat. no. C737303), per the manufacturer's
191 instructions, and plasmid DNA subsequently was isolated using a QIAGEN Plasmid Maxi Kit
192 (cat. no. 12162), per the manufacturer's instructions. This plasmid then was transfected into
193 Takara's Lenti-X™ 293T cells (Clontech, cat. no. 632180), using Takara's Xfect™ Transfection
194 Reagent (Clontech, cat. no. 631317), per the manufacturer's instructions, to generate infectious
195 lentiviral particles that would direct expression of AcGFP1, KRAS^{G12D}, and p53^{R167H} mutants in
196 transduced cells.
197

198 # Generation of shRNA-expressing vectors

199 Short hairpin RNA (shRNA) constructs targeting the porcine SMAD4 and p16 genes
200 were created using InvivoGen's siRNA Wizard™ software (www.invivogen.com/sirnawizard).

201 Three targeting sequences for each gene along with scrambled controls initially were generated
202 and tested. The shRNA construct that demonstrated the best target knock-down in preliminary
203 experimentation (as verified by PCR, data not shown) was utilized for subsequent experiments
204 (see Table S3 for sequences ultimately selected for the shRNA constructs). Primers were cloned
205 into the psiRNA-h7SKhygro G1 and psiRNA-h7SKneo G1 vectors (InvivoGen, cat. no. ksirna3-
206 h21 and ksirna3-n21, respectively; www.invivogen.com) and plasmids then were isolated, all per
207 the manufacturer's protocol.
208

209 # Cell transformations

210 Primary porcine pancreatic epithelial cells in T75 flasks were grown to 80% confluency
211 under standard conditions. The media then was exchanged with 2-3 mL of supernatant from non-
212 lysed Lenti-X™ 293T cells (containing GKP viral particles) with 2 µg/mL polybrene (cat. no.
213 TR1003, Thermo Fisher Scientific). After 24-48 h at 37˚C, treated epithelial cells were re-seeded
214 into 6-well plates under standard conditions and grown to 80% confluency. An exchange with
215 whole media containing 2 µg/mL G418 aminoglycoside antibiotic then was performed; the G418
216 dose was chosen based on preliminary dose-response studies against non-treated epithelial cells.
217 After 24 h, a whole media exchange was done, and the presence of transduced cells was
218 determined with inverted GFP fluorescent microscopy of living cells. Subsequent transfections
219 for RNAi were done with the above plasmids employing shRNA sequences against SMAD4
220 and/or p16, and using the LyoVec™ reagent (InvivoGen, cat. no. lyec-12), all per the
221 manufacturer's protocol. Transfected cells then were selected for expression of the shRNA
222 vector using the appropriate aminoglycoside antibiotic (G418 or hygromycin B).
223

224 # PCR

225 Cell and tissue RNA was isolated using the QIAGEN RNEasy Mini Kit. Purified RNA
226 then was used to generate cDNA using the Verso cDNA Synthesis Kit. The Platinum® Blue
227 PCR Supermix (Invitrogen™/Life Technologies, cat. no. 12580) subsequently was used for all
228 PCR reactions. Amplified products were separated with agarose gel electrophoresis, and then
229 visualized using a UV-light box. qPCR was performed using the PowerUp™ SYBR® Green
230 Master Mix (Applied Biosystems™/ Thermo Fisher Scientific, cat. no. A25741) per
231 manufacturer's protocol, and run on an Applied Biosystems™ 7500 Fast Dx Real-Time PCR
232 Instrument. Fold changes in gene expression were calculated using the comparative C_T method
233 [*30*]. All primers used are listed in Table S3.
234

235 # Immunoblotting

236 Western blot analysis was performed to confirm overexpression of the mutant p53 protein
237 (see Table S4 for a list of antibodies used), as previously described [*31*]. An antibody specific for
238 the mutant KRAS protein was not commercially available. Antibody expression was visualized
239 using the Li-Cor Odyssey Electrophoresis Imaging System (www.licor.com).
240

241 # Soft agar assay

242 A standard soft agar assay [*32*] was used to determine anchorage independent growth. A
243 base layer of 1% agarose was plated into 6-well plates. A total of 2,500 cells/well were mixed
244 with 0.7% agarose and plated on top of the base layer. The plates were incubated under standard
245 conditions for 21 days. The cells then were stained with crystal violet, and counted using an

246 inverted microscope. Cells were plated in triplicate, and total counts from all three wells were
247 averaged.
248

249 Migration assay

250 A standard scratch assay (monolayer wounding) [*33*] was performed to determine cellular
251 migration rate. Cells were plated in triplicate into 6-well plates. A horizontal scratch using a 10
252 µL pipet tip was made in each well. After washing away scratched-off cells, baseline images
253 along the scratch were obtained, the plates were incubated under standard conditions, and
254 subsequent images were captured at 3, 6, 9, 12, and 15 h after the initial scratch. ImageJ software
255 (imagej.nih.gov/ij) was used to measure the distance between the two migrating cellular fronts
256 (scratch edges) at 3-5 locations along the scratch. Average distance at each time point was
257 plotted to generate the migratory rate (µm/h).
258

259 Invasion assay

260 BioCoat™ Matrigel™ Invasion Chambers (Corning™, Thermo Fisher Scientific, cat. no.
261 08-774) were plated with 50,000 cells (upper chamber) in triplicate, and incubated under
262 standard conditions for 24 h. The media from the upper chamber then was removed, and any
263 cells remaining in the upper chamber were removed using a cotton swab. Cells that had migrated
264 to the bottom of the membrane were stained using a Kwik-Diff™ kit (Shandon™, Thermo Fisher
265 Scientific, cat. no. 9990701). Membranes were mounted onto glass slides, and cells per high-
266 power field were counted using ImageJ software.
267

268 Population doubling assay

269 Cells were plated in 6-well plates (20,000 cell/well), and cultured under standard
270 conditions. Triplicate plates then were trypsinized on days 1, 2, 3, 4, 6, and 8, and cells were
271 counted with a hemocytometer. Cell number *vs*. day was plotted to determine the day range in
272 which linear growth was achieved. The data from this linear growth phase were used to
273 determine population doubling time (DT) using the formula: $DT = (\Delta t) \times \ln(2) \div \ln(N_f/N_i)$
274 where Δt = time interval between initial and final cell count, N_f = cell count at final time, and N_i
275 = cell count at initial time.
276

277 # Proliferation assay

278 Relative cell proliferation rates were assayed using an MTT (3-(4,5-dimethylthiazol-2-
279 yl)-2,5-diphenyltetrazolium bromide) assay kit (Vybrant™ MTT Cell Proliferation Assay Kit,
280 Invitrogen™, Thermo Fisher Scientific, cat. no. V13154). Cells were plated in triplicate in a 96-
281 well plate (5,000 cell/well), and cultured under standard conditions for 48 h. MTT reagent then
282 was added to the cells per the manufacturer's instructions, followed by addition of the solvent
283 solution 3.5 h later. Absorbance was measured with a plate reader 3.5 h after solvent addition.
284 Mean absorbance was normalized to absorbance from wild type pancreatic ductal epithelial cells
285 to calculate fold-difference in proliferation.
286

287 # Immunofluorescence and immunohistochemistry

288 Antibodies used in immunofluorescent and immunohistochemical experiments are listed
289 in Table S4. Agilent Dako EnVision kits (www.agilent.com) were used for all IHC analyses per
290 the manufacturer's instructions.
291

292 ## Subcutaneous tumorigenic cell injection

293 Subcutaneous implantation of tumorigenic cells was performed as previously described
294 [*34*], with some modifications. Transformed porcine pancreatic ductal epithelial cells (the three
295 lineages described in Table 1) were trypsinized, counted, and resuspended in DMEM at a
296 concentration of 1×10^7 viable cells/mL. Nude mice (N = 30; 100% female; maintained in
297 microisolator cages with soft bedding and fed regular chow) were randomized into three
298 treatment groups (representing each transformed cell line in Table 1; N = 10 mice per group,
299 100% female) using an online randomization tool. Mice then were injected with 5×10^6 cells
300 (500 μL) into the right hind flank under brief isoflurane inhalational anesthesia, administered
301 with a Matrx VMS® small animal anesthesia machine, within a small animal operating room.
302 Tumors were allowed to grow for 6 weeks or until they reached 2 cm in diameter, as measured
303 with a caliper, and then subjects were euthanized using an AVMA-approved [*28*] method of CO_2
304 asphyxiation. At necropsy all gross tumor was measured and collected, portions underwent
305 formalin fixation and paraffin embedding, and sections subsequently underwent H&E or
306 immunohistochemical staining as described above. An independent, a blinded pathologist
307 analyzed the stained sections to determine whether tumors were epithelial in origin, and if they
308 displayed malignant features.
309

310 ## Orthotopic tumorigenic cell injection

311 Orthotopic implantation of tumorigenic cells was performed as previously described [*34*]
312 to analyze metastases and desmoplasia. In brief, transformed porcine pancreatic ductal epithelial
313 cells (the three lineages described in Table 1) were trypsinized and counted, and 1×10^4 viable
314 cells were suspended into 20 μL DMEM. Nude mice (N = 36; 100% female) housed as described

315 above were randomized into three treatment groups (representing each transformed cell line in
316 Table 1; N = 12 per group, 100% female) using an online randomization tool. The 20 μL cell
317 suspension then was injected with a 20-gauge needle into the pancreas of each nude mouse
318 through a 5 mm incision in the left upper quadrant, under isoflurane anesthesia within a small
319 animal operating room. Mice were euthanized 6 weeks after injection using CO_2 asphyxiation as
320 described above, and tumors and organs were harvested for gross and histologic analysis, as
321 described in the previous paragraph.
322

323 ## Statistics and power analysis

324 Data are reported as mean ± standard deviation. Groups of continuous data were
325 compared with ANOVA and the unpaired t-test. Categorical data were compared with the Fisher
326 or Chi square test. For the power analysis of the murine subcutaneous tumor implant assay,
327 tumor diameter was selected as the endpoint. Setting alpha = 0.05 and power = 0.8, ten mice per
328 group were needed across three groups to detect a difference in means of 30% with the standard
329 deviation estimated at 20% of the mean. In the orthotopic implantation assay, N = 10 mice per
330 treatment group across three treatment groups were needed to detect a 100% difference in effect
331 (+tumor) at a single metastatic site (with alpha set at 0.05 and power = 0.8); or, combining all
332 seven metastatic sites together, N = 10 mice per group were needed to detect a 40% difference in
333 effect.

Results

Isolation of primary porcine pancreatic ductal epithelial cells

Cells cultured from micro-dissected pancreatic ducts displayed epithelial morphology under phase microscopy and stained for CK19 (an established marker of pancreatic ductal epithelium [*35*]; **Fig. 1A-B**). Based on these results, we were confident that we had a population of pancreatic epithelial cells that we could use to generate tumorigenic cell lines.

Generation of tumorigenic cell lines

In order to transform our primary porcine pancreatic ductal epithelial cells, we first generated a lentiviral construct containing *KRAS*^{G12D} and *TP53*^{R167H}, genes previously identified [*29*] as the porcine equivalents to the mutant *KRAS* and *TP53* which are present in multiple human cancers [*36-40*]; in the mouse, expression of these mutants was the basis for the KRAS/p53 genetically engineered murine model of pancreatic cancer [*41*]. For our model, we chose to use a lentiviral platform for the vector, because its genome would be large enough to accommodate insertion of both mutant genes; in addition, we believed that a lentivirus would be optimal for transforming primary cells.

Since initial sequencing of the porcine genome has been accomplished [*42*], we were able to utilize the National Library of Medicine's nucleotide BLAST® database (blast.ncbi.nlm.nih.gov/blast.cgi) to determine the porcine genetic equivalents for human *SMAD4* and *CDKN2A*. We then designed primers (Table S3) to amplify these two genes from genomic DNA isolated from skin of a healthy domestic pig. We sequenced our amplification products,

356 and accessed the BLAST® database to confirm that our products aligned with the porcine
357 *SMAD4* and *CDKN2A* gene sequences. We then proceeded to generate lentiviral constructs to
358 transform primary porcine pancreatic ductal epithelial cells into cell lines expressing various
359 combinations of mutant KRAS and p53, SMAD4 shRNA, and $p16^{Ink4A}$ shRNA (see cell line
360 definitions in Table 1), as described under Materials and Methods.

361 Primary porcine epithelial cells next were transduced with the GKP lentivirus to generate
362 transformed cell lines. Overexpression of $KRAS^{G12D}$ and $p53^{R167H}$ was confirmed in these cell
363 lines with qPCR and immunoblotting (**Fig. 1C-E**). Of note, we could not obtain a reliable
364 antibody to detect porcine KRAS with immunoblotting, so we had to rely on qPCR results and
365 expression of GFP as markers of $KRAS^{G12D}$ expression. Preliminary *in vitro* analyses to probe
366 the tumorigenic properties of these GKP-transformed cell lines demonstrated modest increases in
367 soft agar colony formation and migration speed over wild type cells (**Fig. 2A & B**). Interestingly,
368 the cell line (2.22) with the best performance in the soft agar and migration assays had only
369 modest overexpression of $KRAS^{G12D}$ and $p53^{R167H}$ (**Fig. 1 & 2**); in contrast, the cell lines with
370 the highest mutant overexpression performed relatively poorly in these *in vitro* assays of
371 "tumorigenesis" (i.e., evidence of transformed behavior in cell culture).

372 While *in vitro* experiments were being performed, *in vivo* pancreatic tumor induction was
373 attempted utilizing a transgenic mini-pig available from the NSRRC. Known as the "Oncopig,"
374 [*26*], this subject carries an LSL-cassette containing the dominant negative $TP53^{R167H}$ and the
375 activated $KRAS^{G12D}$ sequences [*26,43,44*]; i.e., this subject is the porcine analog of the
376 KRAS/p53 mouse [*41,45*]. As demonstrated previously, site-specific expression of Cre
377 recombinase in the Oncopig resulted in localized p53 inhibition and KRAS activation, while
378 subcutaneous injection of AdCre produced mesenchymal tumors at the injection sites [*26*]. We

379 injected Cre recombinase into the pancreas of five Oncopigs (**Protocol S2**; **Fig. S2**; **Tables S5**
380 and **S6**). After four months, we observed no gross tumors. However, there was
381 immunohistochemical evidence of transgene expression at the pancreatic injection sites along
382 with numerous microscopic proliferative lesions with desmoplastic features (**Fig. S2**).
383 Based on the modest evidence of *in vitro* transformation and the lack of gross *in vivo*
384 tumorigenesis using expression of $p53^{R167H}$ and $KRAS^{G12D}$ only, we decided that additional
385 oncogenic stress might be helpful to increase the tumor-like properties of transformed pancreatic
386 ductal epithelial cells. Utilizing cell line 2.22 (hereafter referred to PGKP; see Table 1), which
387 had relatively good performance in the soft agar and migration assays (**Fig. 2A & B**), sequential
388 transduction with lentiviral constructs expressing shRNA against SMAD4 and then $p16^{Ink4A}$ was
389 performed to generate cell lines PGKPS and PGKPSC (see Table 1), respectively. RT-PCR then
390 was used to confirm knockdown of the targeted transcripts in these two cell lines (**Fig. 2C**).
391

392 *In vitro* tumorigenic properties of transformed cells

393 The *in vitro* "tumorigenic" properties of the PGKP, PGKPS, and PGKPSC cell lines first
394 were compared with the soft agar and migration assays (**Fig. 2D & E**). Addition of SMAD4 ±
395 $p16^{Ink4A}$ knockdown enhanced the ability of transformed cells to form colonies in soft agar and
396 increased their migration speed (2D wounding assay), particularly when both transcripts were
397 targeted (i.e., the PGKPSC line). We then compared population doubling time, proliferation
398 (metabolic dye conversion) , and Matrigel® invasion ability among the three transformed lines
399 with respect to wild type cells (**Fig. 3A-C**). Both the PGKPS and PGKPSC cell lines had greater
400 proliferation and invasive ability compared to either wild type cells or the PGKP cell line (**Fig.**
401 **3B, C**). The doubling time for all three transformed cell lines was approximately the same at ~15

402 h, compared to the ~4 d doubling time of wild type cells (**Fig. 3A**). Based on the *in vitro* assays
403 of tumorigenesis, we suspected that all three of our transformed cell lines had the potential to
404 form tumors *in vivo*, albeit to varying degrees. We subsequently decided to compare the *in vivo*
405 tumorigenicity among all three cell lines in an immunodeficient mouse model.
406

407 Subcutaneous and orthotopic tumor transplants in immunodeficient 408 mice

409 In order to determine if our cell lines retained their tumorigenic properties *in vivo*, we
410 utilized homozygous athymic mice to generate subcutaneous and orthotopic cell implantation
411 models. The subcutaneous model was used to assess *in vivo* tumor growth. All three cell lines
412 grew sizeable tumors (>1 cm diameter) within 6 weeks; growth rates were not statistically
413 different among the three cell lines (**Fig. 4A & B**). The subcutaneous tumors were well-
414 vascularized and mucinous in gross appearance (**Fig. 4A**). Confirmation of GKP lentiviral
415 transduction was demonstrated with immunohistochemistry of the $p53^{R167H}$ mutant in
416 subcutaneous tumors (**Fig. S3**).
417 Tumors from the subcutaneous implant model then underwent immunohistochemical
418 staining with an array of epithelial and mesenchymal markers (**Fig. 5**). The distribution of
419 staining for the epithelial markers (E-cadherin, epithelial cell adhesion molecule, pan-
420 cytokeratin, cytokeratin-19) generally was more diffuse than the mesenchymal marker staining.
421 In some regions the epithelial marker staining was clustered and intense. The overall abundance
422 of staining for the epithelial markers appeared greater in the PGKPS and PGKPSC lines with
423 respect to the PGKP line. The distribution of staining for the mesenchymal markers (α-smooth
424 muscle actin, vimentin, and type I collagen) was variable, sometimes appearing in cords or

425 strands in some sections, reminiscent of the desmoplastic reaction in human pancreatic cancer
426 [*46,47*]. In other sections, mesenchymal marker staining was minimal. Similar to the epithelial
427 markers, the overall abundance of staining for the mesenchymal markers appeared greater in the
428 PGKPS and PGKPSC lines compared to the PGKP line.

429 With the immunohistochemical studies of the subcutaneous tumors demonstrating some
430 epithelial characteristics, the nude mouse orthotopic implantation model was used next to assess
431 the metastatic potential of all three cell lines. The percentage of mice implanted with each cell
432 line that subsequently developed metastasis in the small bowel, diaphragm, liver, lung, lymph
433 node, peritoneum, or spleen is shown in **Fig. 4C.** The degree of metastatic spread was minimal;
434 nodal tissue was the only metastatic site common to all three lines. The PGKPCS cell line
435 exhibited the greatest array of metastatic spread ($p < 0.002$, Chi-square), with the most common
436 site being the spleen (though it was not clear in two of five mice with splenic disease after
437 PGKPSC implantation whether the spleen was involved with extension from the primary tumor,
438 or from direct seeding, or whether these were true metastases). Interestingly, one of the two
439 subjects with liver metastasis after PGKPSC implantation had primary tumor within the
440 gallbladder, rather than within the pancreas. Similar to the subcutaneous tumor model, most
441 tumors in the orthotopic model were well-vascularized and mucinous in gross appearance.
442
443

Discussion

Our overall goal with this project was to generate tumorigenic pancreatic cell lines that could be used in an immunocompetent porcine model of pancreatic cancer. Current murine models for pancreatic cancer will continue to be helpful, particularly for the study of molecular mechanisms. However, murine models are limited in their ability to replicate human biology and size, so a large animal model of pancreatic cancer likely would enhance our ability to develop and test new diagnostic and treatment modalities for this disease. The data presented herein demonstrated that wild type porcine pancreatic ductal epithelium can be transformed with modulation of common tumor-associated target genes, and that these transformed cells subsequently can grow tumors in immunodeficient mice. These data provide a pathway for the construction of an autochthonous porcine model of pancreatic cancer, namely, orthotopic implantation of tumorigenic pancreatic cells. Proof-of-principle for tumor growth in pigs using subcutaneous implantation of *ex-vivo* transformed autologous fibroblasts was demonstrated in 2007 [*29*].

Porcine biomedical models have been used for decades in the fields of trauma and hemostasis [*48*], xenotransplantation [*49,50*], dermal healing [*51*], toxicology [*52*], atherosclerosis [*53*], and cardiac regeneration [*54*]; the utility of these models is growing. A porcine genome map was generated in 2012 [*42*], and further coverage, annotation, and confirmation is ongoing [*55,56*]. Porcine-centered online tools and databases are now available [*57*]. Genetic manipulation of pigs (including knockouts, tissue-specific transgenics, inducible expression [*29,58-65*]) with similar tools as used in the mouse is becoming more routine, with

467 new gene-edited porcine models emerging in 2015-2017 for diseases such as atherosclerosis,
468 cystic fibrosis, Duchenne muscular dystrophy, and ataxia telangiectasia [*44,66,67*].
469 The rationale to build a porcine model of pancreatic cancer is (1) to have a platform for
470 diagnostic/therapeutic device development otherwise not achievable in murine models; and (2) to
471 have a highly predictive preclinical model in which anti-cancer therapies (including
472 immunotherapies) could be vetted/optimized prior to a clinical trial [*68*]. The rationale to use the
473 pig in this modeling effort is that this species mimics human genomics [*55,69-72*], epigenetics
474 [*73*], physiology [*52,69,74,75*], metabolism [*69,75,76*], inflammation and immune response
475 [*72,77-81*], and size [*75,82*] remarkably well (in particular, better than mice), with reasonable
476 compromises towards cost and husbandry [*75*]. So based on the pig's relatively large size and its
477 proven track record in replicating human biology which, incidentally, is a demonstrably better
478 replication than can be obtained with rodents, we selected swine as the model organism for this
479 pancreatic cancer project.
480 Research on immunocompetent large animal cancer models [*83-85*] includes prostate
481 cancer, for which there is a canine model [*86*]. In addition, in 2012 a group in Munich reported
482 the engineering of (i) an *APC* mutant pig that developed rectal polyposis [*16,87*] and (ii) a pig
483 with Cre-inducible p53 deficiency [*63*]. This group subsequently determined that their p53-null
484 subjects ($TP53^{R167H/R167H}$) developed osteosarcoma by age 7-8 months [*88*]. Other p53-deficient
485 pigs have been engineered since this initial report [*64,89*]; in the report from Iowa, half (5 out of
486 10) of p53-deficient ($TP53^{R167H/R167H}$) pigs developed lymphoma or osteogenic tumor at age 6-18
487 months [*64*]. A group in Denmark reported the creation of a *BRCA* mutant pig in 2012. [*90*].
488 A KRAS/p53 "Oncopig" was reported in 2015 [*26,43,44,84*]. This subject has a somatic
489 LSL-cassette that can express dominant negative p53 (R167H mutation) and activated KRAS

490 (G12D mutation); i.e., the porcine analog of the KRAS/p53 mouse [*41,45*]. Site-specific
491 expression of Cre recombinase in the Oncopig resulted in localized p53 inhibition and KRAS
492 activation; subcutaneous injection of AdCre produced mesenchymal tumors at the injection sites
493 [*26*]. In 2017, initial work was published on a Oncopig-based model of hepatocellular carcinoma
494 [*91*]. Also in 2017, another genetic porcine model of intestinal neoplasia was reported [*92*],
495 utilizing inducible expression of $KRAS^{G12D}$, c-Myc, SV40 large T antigen, and retinoblastoma
496 protein (pRb). One out of three pigs total in this model developed duodenal neuroendocrine
497 carcinoma with lymph node metastasis at two months after induction. A porcine model of
498 pancreatic cancer has not yet been reported, other than some preliminary data presented by us in
499 2017 [*93*].

500 The process we used for developing transformed porcine pancreatic ductal epithelial cell
501 lines for future orthotopic implantation was somewhat iterative, in that we modified our strategy
502 along the way based on our early results. Commonly mutated genes in pancreatic cancer include
503 *KRAS* [*94,95*] and *TP53* [*95-97*]. In mice, somatic activation of KRAS via the G12D mutation
504 ($KRAS^{G12D}$) produced widely metastatic pancreatic tumors; survival duration in these subjects
505 decreased further with p53 inactivation [*41*]. Based on this murine model, and the published
506 success with subcutaneous tumor induction in the KRAS/p53 Oncopig [*26*], we elected to
507 transform pancreatic ductal epithelial cells with expression of activated $KRAS^{G12D}$ and $p53^{R167H}$
508 only. However, the initial results from our *in vitro* transformation assays with these two gene
509 edits (i.e., the PGKP cell line of Table 1) were somewhat underwhelming. Combined with the
510 finding of no gross tumor four months after pancreatic AdCre injection in five Oncopig subjects,
511 we decided that additional genetic "hits" might be necessary for transformation of porcine
512 pancreatic ductal epithelial cells. Of note, Schook et al. [*29*] found that porcine dermal

513 fibroblasts required six genetic edits (human telomerase reverse transcriptase, dominant negative
514 p53, cyclin D1, activated cyclin dependent kinase, oncogenic c-Myc, and oncogenic H-Ras) to
515 optimize the tumorigenic phenotype of this particular cell.

516 Other commonly mutated genes in pancreatic cancer include *SMAD4* [*95,98*] and
517 *CDKN2A* [*95,99*]. Deletion of *SMAD4* or *CDKN2A* in a *KRAS*^{G12D} murine pancreatic cancer
518 model enhanced tumor growth [*100,101*]. Based on these published data and our above
519 transformation results with just the *KRAS* and *TP53* edits, we elected to add knockdown of
520 SMAD4 and p16 to our list of hits for transformation of porcine pancreatic ductal epithelial cells.
521 Ultimately, all three of our cell lines (Table 1) demonstrated transformed behavior *in vitro* and
522 the ability to form tumors *in vivo* (nude mice), with perhaps some enhancement by the addition
523 of SMAD4 and p16 knockdown. In the future, we intend to utilize CRISPR/Cas9 editing to
524 disrupt the genes of these and/or other targets.

525 Although we utilized a relatively high number of cells to obtain tumor formation in our
526 nude mice experiments, we feel that this is due to the relative young age of our cell lines, which
527 did not undergo as many passages as other cell lines which have been used to study pancreatic
528 cancer. Thus, the transformed cell lines in this report likely did not undergo an inadvertent
529 selection for the fastest growing cells, as may occur in older, extensively-passaged lines.
530 Regarding the lack of desmoplasia in our murine xenograft model, we did not consider this
531 surprising, in that most immunodeficient murine models of pancreatic cancer do not recapitulate
532 the extent of desmoplasia or metastasis seen with human disease. We anticipate that future
533 experiments involving the implantation of transformed pancreatic ductal epithelial cells into wild
534 type swine (and thus into a "normal" microenvironment with "normal" immunoediting) will
535 produce tumors with desmoplasia and metastasis.

536 Of note, the pathologic findings in our five Oncopig subjects, while not macroscopically
537 tumorous, displayed tissue architecture reminiscent of desmoplasia. Regarding the lack of
538 macroscopic tumor in these transgenic pigs, it is conceivable that the induction process was not
539 optimal secondary to an inadequate dose of AdCre, inadequate recombinase activity, inadequate
540 tissue delivery of the enzyme, or some other technical issue. Our future plans in this respect will
541 involve additional attempts at induction of pancreatic tumor in the Oncopig with and without
542 introduction of some additional gene edits, such as local disruption of *SMAD4* and *CDKN2A*
543 (e.g., with *in vivo* CRISPR/Cas9 gene editing [*102,103*]).

544 # References

545 1. American Cancer Society. *Cancer Facts & Figures 2016*. Atlanta: American Cancer
546 Society; 2016. Available from:
547 http://www.cancer.org/research/cancerfactsstatistics/cancerfactsfigures2016/index.
548 2. *SEER (Surveillance, Epidemiology, and End Results Program) Stat Fact Sheets:*
549 *Pancreas Cancer*. National Cancer Institute. Accessed December 12, 2016. URL:
550 http://seer.cancer.gov/statfacts/html/pancreas.html.
551 3. National Comprehensive Cancer Network. Pancreatic Adenocarcinoma, Version 1.2018.
552 In: NCCN Clinical Practice Guidelines In Oncology (NCCN Guidelines®). NCCN; 27
553 April 2018. Available from: www.nccn.org.
554 4. Seok J, Warren HS, Cuenca AG, Mindrinos MN, Baker HV, Xu W, et al. Genomic
555 responses in mouse models poorly mimic human inflammatory diseases. *PNAS* 2013;
556 110(9): 3507-12. PMID: 23401516. doi: 10.1073/pnas.1222878110.
557 5. Begley CG, Ellis LM. Drug development: Raise standards for preclinical cancer research.
558 *Nature* 2012; 483(7391): 531-3. PMID: 22460880. doi: 10.1038/483531a.
559 6. Cook N, Jodrell DI, Tuveson DA. Predictive in vivo animal models and translation to
560 clinical trials. *Drug Discov Today* 2012; 17(5-6): 253-60. PMID: 22493784. doi:
561 10.1016/j.drudis.2012.02.003.
562 7. Le Magnen C, Dutta A, Abate-Shen C. Optimizing mouse models for precision cancer
563 prevention. *Nat Rev Cancer* 2016; 16(3): 187-96. PMID: 26893066. doi:
564 10.1038/nrc.2016.1.

565 8. Reichert JM, Wenger JB. Development trends for new cancer therapeutics and vaccines.
566 *Drug Discov Today* 2008; 13(1-2): 30-7. PMID: 18190861. doi:
567 10.1016/j.drudis.2007.09.003.
568 9. Sharpless NE, Depinho RA. The mighty mouse: genetically engineered mouse models in
569 cancer drug development. *Nat Rev Drug Discov* 2006; 5(9): 741-54. PMID: 16915232.
570 doi: 10.1038/nrd2110.
571 10. Ebos JM, Kerbel RS. Antiangiogenic therapy: impact on invasion, disease progression,
572 and metastasis. *Nat Rev Clin Oncol* 2011; 8(4): 210-21. PMID: 21364524. doi:
573 10.1038/nrclinonc.2011.21.
574 11. Francia G, Cruz-Munoz W, Man S, Xu P, Kerbel RS. Mouse models of advanced
575 spontaneous metastasis for experimental therapeutics. *Nat Rev Canc* 2011; 11(2): 135-41.
576 PMID: 21258397. doi: doi:10.1038/nrc3001.
577 12. O'Collins VE, Macleod MR, Donnan GA, Horky LL, van der Worp BH, Howells DW.
578 1,026 experimental treatments in acute stroke. *Ann Neurol* 2006; 59(3): 467-77. PMID:
579 16453316. doi: 10.1002/ana.20741.
580 13. Scott S, Kranz JE, Cole J, Lincecum JM, Thompson K, Kelly N, et al. Design, power,
581 and interpretation of studies in the standard murine model of ALS. *Amyotroph Lat Scler*
582 2008; 9(1): 4-15. PMID: 18273714. doi: 10.1080/17482960701856300.
583 14. Talmadge JE, Singh RK, Fidler IJ, Raz A. Murine models to evaluate novel and
584 conventional therapeutic strategies for cancer. *Am J Pathol* 2007; 170(3): 793-804.
585 PMID: 17322365. doi: 10.2353/ajpath.2007.060929.

586 15. Rogers CS, Stoltz DA, Meyerholz DK, Ostedgaard LS, Rokhlina T, Taft PJ, et al.
587 Disruption of the CFTR gene produces a model of cystic fibrosis in newborn pigs.
588 *Science* 2008; 321(5897): 1837-41. PMID: 18818360. doi: 10.1126/science.1163600.
589 16. Flisikowska T, Merkl C, Landmann M, Eser S, Rezaei N, Cui X, et al. A porcine model
590 of familial adenomatous polyposis. *Gastroenterology* 2012; 143: 1173-5. PMID:
591 22864254. doi: 10.1053/j.gastro.2012.07.110.
592 17. Pezzulo AA, Tang XX, Hoegger MJ, Abou Alaiwa MH, Ramachandran S, Moninger TO,
593 et al. Reduced airway surface pH impairs bacterial killing in the porcine cystic fibrosis
594 lung. *Nature* 2012; 487(7405): 109-13. PMID: 22763554. doi: 10.1038/nature11130.
595 18. Maddalo D, Manchado E, Concepcion CP, Bonetti C, Vidigal JA, Han YC, et al. In vivo
596 engineering of oncogenic chromosomal rearrangements with the CRISPR/Cas9 system.
597 *Nature* 2014; 516(7531): 423-7. PMID: 25337876. doi: 10.1038/nature13902.
598 19. Sanchez-Rivera FJ, Papagiannakopoulos T, Romero R, Tammela T, Bauer MR, Bhutkar
599 A, et al. Rapid modelling of cooperating genetic events in cancer through somatic
600 genome editing. *Nature* 2014; 516(7531): 428-31. PMID: 25337879. doi:
601 10.1038/nature13906.
602 20. Day CP, Merlino G, Van Dyke T. Preclinical mouse cancer models: a maze of
603 opportunities and challenges. *Cell* 2015; 163(1): 39-53. PMID: 26406370. doi:
604 10.1016/j.cell.2015.08.068.
605 21. Singh M, Murriel CL, Johnson L. Genetically engineered mouse models: closing the gap
606 between preclinical data and trial outcomes. *Cancer Res* 2012; 72(11): 2695-700. PMID:
607 22593194. doi: 10.1158/0008-5472.CAN-11-2786.

608 22. Zitvogel L, Pitt JM, Daillere R, Smyth MJ, Kroemer G. Mouse models in
609 oncoimmunology. *Nat Rev Cancer* 2016; 16(12): 759-73. PMID: 27687979. doi:
610 10.1038/nrc.2016.91.
611 23. Kilkenny C, Browne WJ, Cuthill IC, Emerson M, Altman DG. Improving bioscience
612 research reporting: the ARRIVE guidelines for reporting animal research. *PLoS Biol*
613 2010; 8(6): e1000412. PMID: 20613859. doi: 10.1371/journal.pbio.1000412.
614 24. National Institutes of Health. *Principles and Guidelines for Reporting Preclinical*
615 *Research*. Accessed 5 February 2016. https://www.nih.gov/research-training/rigor-
616 reproducibility/principles-guidelines-reporting-preclinical-research.
617 25. National Institutes of Health. *Enhancing Reproducibility through Rigor and*
618 *Transparency*. NOT-OD-15-103. June 9, 2015. http://grants.nih.gov/grants/guide/notice-
619 files/NOT-OD-15-103.html
620 26. Schook LB, Collares TV, Hu W, Liang Y, Rodrigues FM, Rund LA, et al. A Genetic
621 Porcine Model of Cancer. *PLOS ONE* 2015; 10(7): e0128864. PMID: 26132737. doi:
622 10.1371/journal.pone.0128864.
623 27. Committee for the Update of the Guide for the Care and Use of Laboratory Animals.
624 *Guide for the Care and Use of Laboratory Animals*. Washington, DC: The National
625 Academies Press; 2011.
626 28. American Veterinary Medical Association Panel on Euthanasia. *AVMA Guidelines for the*
627 *Euthanasia of Animals*. Schaumberg, IL: American Veterinary Medical Association;
628 2013.

629 29. Adam SJ, Rund LA, Kuzmuk KN, Zachary JF, Schook LB, Counter CM. Genetic
630 induction of tumorigenesis in swine. *Oncogene* 2007; 26(7): 1038-45. PMID: 16964292.
631 doi: 10.1038/sj.onc.1209892.
632 30. Schmittgen TD, Livak KJ. Analyzing real-time PCR data by the comparative C(T)
633 method. *Nat Protoc* 2008; 3(6): 1101-8. PMID: 18546601. doi:
634 31. Grinnell F, Zhu M, Carlson MA, Abrams JM. Release of mechanical tension triggers
635 apoptosis of human fibroblasts in a model of regressing granulation tissue. *Exp Cell Res*
636 1999; 248(2): 608-19. PMID: 10222153. doi: 10.1006/excr.1999.4440.
637 32. Macpherson I, Montagnier L. Agar Suspension Culture for the Selective Assay of Cells
638 Transformed by Polyoma Virus. *Virology* 1964; 23: 291-4. PMID: 14187925. doi:
639 33. Liang CC, Park AY, Guan JL. In vitro scratch assay: a convenient and inexpensive
640 method for analysis of cell migration in vitro. *Nat Protoc* 2007; 2(2): 329-33. PMID:
641 17406593. doi: 10.1038/nprot.2007.30.
642 34. Tsutsumida H, Swanson BJ, Singh PK, Caffrey TC, Kitajima S, Goto M, et al. RNA
643 interference suppression of MUC1 reduces the growth rate and metastatic phenotype of
644 human pancreatic cancer cells. *Clin Cancer Res* 2006; 12(10): 2976-87. PMID:
645 16707592. doi: 10.1158/1078-0432.CCR-05-1197.
646 35. Gioviale MC, Damiano G, Montalto G, Buscemi G, Romano M, Lo Monte AI. Isolation
647 and culture of beta-like cells from porcine Wirsung duct. *Transplant Proc* 2009; 41(4):
648 1363-6. PMID: 19460560. doi: 10.1016/j.transproceed.2009.02.062.
649 36. Govindan R, Ding L, Griffith M, Subramanian J, Dees ND, Kanchi KL, et al. Genomic
650 landscape of non-small cell lung cancer in smokers and never-smokers. *Cell* 2012;
651 150(6): 1121-34. PMID: 22980976. doi: 10.1016/j.cell.2012.08.024.

652 37. Kandoth C, McLellan MD, Vandin F, Ye K, Niu B, Lu C, et al. Mutational landscape and
653 significance across 12 major cancer types. *Nature* 2013; 502(7471): 333-9. PMID:
654 24132290. doi: 10.1038/nature12634.
655 38. Stephens PJ, Tarpey PS, Davies H, Van Loo P, Greenman C, Wedge DC, et al. The
656 landscape of cancer genes and mutational processes in breast cancer. *Nature* 2012;
657 486(7403): 400-4. PMID: 22722201. doi:
658 39. Vogelstein B, Papadopoulos N, Velculescu VE, Zhou S, Diaz LA, Jr., Kinzler KW.
659 Cancer genome landscapes. *Science* 2013; 339(6127): 1546-58. PMID: 23539594. doi:
660 10.1126/science.1235122.
661 40. Waddell N, Pajic M, Patch AM, Chang DK, Kassahn KS, Bailey P, et al. Whole genomes
662 redefine the mutational landscape of pancreatic cancer. *Nature* 2015; 518: 495-501.
663 PMID: PMC4523082. doi: 10.1038/nature14169.
664 41. Hingorani SR, Wang L, Multani AS, Combs C, Deramaudt TB, Hruban RH, et al.
665 Trp53R172H and KrasG12D cooperate to promote chromosomal instability and widely
666 metastatic pancreatic ductal adenocarcinoma in mice. *Cancer Cell* 2005; 7(5): 469-83.
667 PMID: 15894267. doi: 10.1016/j.ccr.2005.04.023.
668 42. Groenen MA, Archibald AL, Uenishi H, Tuggle CK, Takeuchi Y, Rothschild MF, et al.
669 Analyses of pig genomes provide insight into porcine demography and evolution. *Nature*
670 2012; 491(7424): 393-8. PMID: 23151582. doi: 10.1038/nature11622.
671 43. Rodrigues F, Hu W, Rund L, Liang Y, Counter C, Schook L. Development of the "Onco-
672 Pig": An Inducible Transgenic Porcine Model for Human Cancer [poster]. 2013
673 Brazilian Genetics Conference; URL:

674 http://www.dbs.illinois.edu/comparativegenomics/userfiles/file/ocnopigPoster_Brazilian
675 %20Genetics%20Conference2013.pdf.
676 44. Conference Proceedings: Swine in Biomedical Research. July 6-8, 2014. Raleigh, NC.
677 45. DuPage M, Dooley AL, Jacks T. Conditional mouse lung cancer models using adenoviral
678 or lentiviral delivery of Cre recombinase. *Nat Protoc* 2009; 4(7): 1064-72. PMID:
679 19561589. doi: 10.1038/nprot.2009.95.
680 46. Bailey JM, Swanson BJ, Hamada T, Eggers JP, Singh PK, Caffery T, et al. Sonic
681 hedgehog promotes desmoplasia in pancreatic cancer. *Clin Cancer Res* 2008; 14(19):
682 5995-6004. PMID: 18829478. doi: 10.1158/1078-0432.CCR-08-0291.
683 47. Handra-Luca A, Hong SM, Walter K, Wolfgang C, Hruban R, Goggins M. Tumour
684 epithelial vimentin expression and outcome of pancreatic ductal adenocarcinomas. *Br J*
685 *Cancer* 2011; 104(8): 1296-302. PMID: 21448168. doi: 10.1038/bjc.2011.93.
686 48. Kheirabadi BS, Mace JE, Terrazas IB, Fedyk CG, Estep JS, Dubick MA, et al. Safety
687 evaluation of new hemostatic agents, smectite granules, and kaolin-coated gauze in a
688 vascular injury wound model in swine. *J Trauma* 2010; 68(2): 269-78. PMID: 20154537.
689 doi: 10.1097/TA.0b013e3181c97ef1.
690 49. Cooper DK, Ekser B, Ramsoondar J, Phelps C, Ayares D. The role of genetically
691 engineered pigs in xenotransplantation research. *J Pathol* 2016; 238(2): 288-99. PMID:
692 26365762. doi: 10.1002/path.4635.
693 50. Niu D, Wei HJ, Lin L, George H, Wang T, Lee IH, et al. Inactivation of porcine
694 endogenous retrovirus in pigs using CRISPR-Cas9. *Science* 2017; 357(6357): 1303-7.
695 PMID: 28798043. doi: 10.1126/science.aan4187.

696 51. Sullivan TP, Eaglstein WH, Davis SC, Mertz P. The pig as a model for human wound
697 healing. *Wound Repair Regen* 2001; 9(2): 66-76. PMID: 11350644. doi: 10.1046/j.1524-
698 475x.2001.00066.x.
699 52. Swindle MM, Makin A, Herron AJ, Clubb FJ, Jr., Frazier KS. Swine as models in
700 biomedical research and toxicology testing. *Vet Pathol* 2012; 49(2): 344-56. PMID:
701 21441112. doi: 10.1177/0300985811402846.
702 53. Xiangdong L, Yuanwu L, Hua Z, Liming R, Qiuyan L, Ning L. Animal models for the
703 atherosclerosis research: a review. *Protein Cell* 2011; 2(3): 189-201. PMID: 21468891.
704 doi: 10.1007/s13238-011-1016-3.
705 54. Gouadon E, Moore-Morris T, Smit NW, Chatenoud L, Coronel R, Harding SE, et al.
706 Concise Review: Pluripotent Stem Cell-Derived Cardiac Cells, A Promising Cell Source
707 for Therapy of Heart Failure: Where Do We Stand? *Stem Cells* 2016; 34(1): 34-43.
708 PMID: 26352327. doi: 10.1002/stem.2205.
709 55. Walters E, Wolf E, Whyte J, Mao J, Renner S, Nagashima H, et al. Completion of the
710 swine genome will simplify the production of swine as a large animal biomedical model.
711 *BMC Med Genom* 2012; 5(1): 55. PMID: 23151353. doi: 10.1186/1755-8794-5-55.
712 56. Schook LB, Collares TV, Darfour-Oduro KA, De AK, Rund LA, Schachtschneider KM,
713 et al. Unraveling the swine genome: implications for human health. *Annu Rev Anim*
714 *Biosci* 2015; 3: 219-44. PMID: 25689318. doi: 10.1146/annurev-animal-022114-110815.
715 57. Dawson HD, Chen C, Gaynor B, Shao J, Urban JF, Jr. The porcine translational research
716 database: a manually curated, genomics and proteomics-based research resource. *BMC*
717 *Genomics* 2017; 18(1): 643. PMID: 28830355. doi: 10.1186/s12864-017-4009-7.

718 58. Gun G, Kues WA. Current progress of genetically engineered pig models for biomedical
719 research. *Biores Open Access* 2014; 3(6): 255-64. PMID: 25469311. doi:
720 10.1089/biores.2014.0039.
721 59. Fan N, Lai L. Genetically modified pig models for human diseases. *J Genet Genomics*
722 2013; 40(2): 67-73. PMID: 23439405. doi: 10.1016/j.jgg.2012.07.014.
723 60. Prather RS, Lorson M, Ross JW, Whyte JJ, Walters E. Genetically engineered pig models
724 for human diseases. *Annu Rev Anim Biosci* 2013; 1: 203-19. PMID: 25387017. doi:
725 10.1146/annurev-animal-031412-103715.
726 61. Luo Y, Li J, Liu Y, Lin L, Du Y, Li S, et al. High efficiency of BRCA1 knockout using
727 rAAV-mediated gene targeting: developing a pig model for breast cancer. *Transgenic Res*
728 2011; 20(5): 975-88. PMID: 21181439. doi: 10.1007/s11248-010-9472-8.
729 62. Luo Y, Bolund L, Sorensen CB. Pig gene knockout by rAAV-mediated homologous
730 recombination: comparison of BRCA1 gene knockout efficiency in Yucatan and
731 Gottingen fibroblasts with slightly different target sequences. *Transgenic Res* 2012;
732 21(3): 671-6. PMID: 22020980. doi: 10.1007/s11248-011-9563-1.
733 63. Leuchs S, Saalfrank A, Merkl C, Flisikowska T, Edlinger M, Durkovic M, et al.
734 Inactivation and inducible oncogenic mutation of p53 in gene targeted pigs. *PLoS ONE*
735 2012; 7(10): e43323. PMID: 23071491. doi: 10.1371/journal.pone.0043323.
736 64. Sieren JC, Meyerholz DK, Wang XJ, Davis BT, Newell JD, Jr., Hammond E, et al.
737 Development and translational imaging of a TP53 porcine tumorigenesis model. *J Clin*
738 *Invest* 2014; 124(9): 4052-66. PMID: 25105366. doi: 10.1172/JCI75447.

739 65. Yang L, Guell M, Niu D, George H, Lesha E, Grishin D, et al. Genome-wide inactivation
740 of porcine endogenous retroviruses (PERVs). *Science* 2015; 350(6264): 1101-4. PMID:
741 26456528. doi: 10.1126/science.aad1191.
742 66. Beraldi R, Meyerholz D, Savinov A, Kovács A, Weimer J, Dykstra J, et al. Genetic
743 Ataxia Telangiectasia porcine model phenocopies the multisystemic features of the
744 human disease. *Biochim Biophys Acta* 2017: ePub ahead of print, 2017 Jul 23. PMID:
745 28746835. doi: 10.1016/j.bbadis.2017.07.020.
746 67. Perleberg C, Kind A, Schnieke A. Genetically engineered pigs as models for human
747 disease. *Dis Model Mech* 2018; 11(1): dmm030783. PMID: 29419487. doi:
748 10.1242/dmm.030783.
749 68. Segatto NV, Remiao MH, Schachtschneider KM, Seixas FK, Schook LB, Collares T. The
750 Oncopig Cancer Model as a Complementary Tool for Phenotypic Drug Discovery. *Front*
751 *Pharmacol* 2017; 8: 894. PMID: 29259556. doi: 10.3389/fphar.2017.00894.
752 69. Kuzmuk KN, Schook LB. Pigs as a Model for Biomedical Sciences. In: Rothschild MF,
753 Ruvinsky A, editors. *The Genetics of the Pig*. Oxfordshire, UK: CABI; 2011. p. 426-44.
754 70. Emes RD, Goodstadt L, Winter EE, Ponting CP. Comparison of the genomes of human
755 and mouse lays the foundation of genome zoology. *Hum Mol Genet* 2003; 12(7): 701-9.
756 PMID: 12651866. doi: 10.1093/hmg/ddg078.
757 71. Dawson HD, McAnulty P, Dayan A, Ganderup N, Hastings K. A comparative assessment
758 of the pig, mouse and human genomes. In: McAnulty P, Dayan A, Ganderup N, Hastings
759 K, editors. The Minipig in Biomedical Research. Boca Raton, FL: CRC Press; 2012. p.
760 323-42.

761 72. Dawson HD, Smith AD, Chen C, Urban JF, Jr. An in-depth comparison of the porcine,
762 murine and human inflammasomes; lessons from the porcine genome and transcriptome.
763 *Vet Microbiol* 2017; 202: 2-15. PMID: 27321134. doi: 10.1016/j.vetmic.2016.05.013.
764 73. Schachtschneider KM, Madsen O, Park C, Rund LA, Groenen MA, Schook LB. Adult
765 porcine genome-wide DNA methylation patterns support pigs as a biomedical model.
766 *BMC Genomics* 2015; 16: 743. PMID: 26438392. doi: 10.1186/s12864-015-1938-x.
767 74. Vodicka P, Smetana K, Jr., Dvorankova B, Emerick T, Xu YZ, Ourednik J, et al. The
768 miniature pig as an animal model in biomedical research. *Ann N Y Acad Sci* 2005; 1049:
769 161-71. PMID: 15965115. doi: 10.1196/annals.1334.015.
770 75. Swindle MM, Smith AC. *Swine in the Laboratory: Surgery, Anesthesia, Imaging, and*
771 *Experimental Techniques*. 3rd ed. Boca Raton, FL: CRC Press; 2016.
772 76. Spurlock ME, Gabler NK. The development of porcine models of obesity and the
773 metabolic syndrome. *J Nutr* 2008; 138(2): 397-402. PMID: 18203910. doi:
774 77. Röthkotter HJ. Anatomical particularities of the porcine immune system--a physician's
775 view. *Dev Comp Immunol* 2009; 33(3): 267-72. PMID: 18775744. doi:
776 10.1016/j.dci.2008.06.016.
777 78. Bailey M. The mucosal immune system: recent developments and future directions in the
778 pig. *Dev Comp Immunol* 2009; 33(3): 375-83. PMID: 18760299. doi:
779 10.1016/j.dci.2008.07.003.
780 79. Fairbairn L, Kapetanovic R, Sester DP, Hume DA. The mononuclear phagocyte system
781 of the pig as a model for understanding human innate immunity and disease. *J Leukoc*
782 *Biol* 2011; 89(6): 855-71. PMID: 21233410. doi: 10.1189/jlb.1110607.

783 80. Meurens F, Summerfield A, Nauwynck H, Saif L, Gerdts V. The pig: a model for human
784 infectious diseases. *Trends Microbiol* 2012; 20(1): 50-7. PMID: 22153753. doi:
785 10.1016/j.tim.2011.11.002.
786 81. Petersen B, Carnwath JW, Niemann H. The perspectives for porcine-to-human
787 xenografts. *Comp Immunol Microbiol Infect Dis* 2009; 32(2): 91-105. PMID: 18280567.
788 doi: 10.1016/j.cimid.2007.11.014.
789 82. Ferrer J, Scott WE, 3rd, Weegman BP, Suszynski TM, Sutherland DE, Hering BJ, et al.
790 Pig pancreas anatomy: implications for pancreas procurement, preservation, and islet
791 isolation. *Transplantation* 2008; 86(11): 1503-10. PMID: 19077881. doi:
792 10.1097/TP.0b013e31818bfda1.
793 83. Flisikowska T, Kind A, Schnieke A. Pigs as models of human cancers. *Theriogenology*
794 2016; 86(1): 433-7. PMID: 27156684. doi: 10.1016/j.theriogenology.2016.04.058.
795 84. Schachtschneider KM, Schwind RM, Newson J, Kinachtchouk N, Rizko M, Mendoza-
796 Elias N, et al. The Oncopig Cancer Model: An Innovative Large Animal Translational
797 Oncology Platform. *Front Oncol* 2017; 7: 190. PMID: 28879168. doi:
798 10.3389/fonc.2017.00190.
799 85. Watson AL, Carlson DF, Largaespada DA, Hackett PB, Fahrenkrug SC. Engineered
800 Swine Models of Cancer. *Front Genet* 2016; 7: 78. PMID: 27242889. doi:
801 10.3389/fgene.2016.00078.
802 86. Ittmann M, Huang J, Radaelli E, Martin P, Signoretti S, Sullivan R, et al. Animal Models
803 of Human Prostate Cancer: The Consensus Report of the New York Meeting of the
804 Mouse Models of Human Cancers Consortium Prostate Pathology Committee. *Canc Res*
805 2013; 73(9): 2718-36. PMID: 23610450. doi: 10.1158/0008-5472.CAN-12-4213.

806 87. Stachowiak M, Flisikowska T, Bauersachs S, Perleberg C, Pausch H, Switonski M, et al.
807 Altered microRNA profiles during early colon adenoma progression in a porcine model
808 of familial adenomatous polyposis. *Oncotarget* 2017; 8(56): 96154-60. PMID: 29221194.
809 doi: 10.18632/oncotarget.21774.
810 88. Saalfrank A, Janssen KP, Ravon M, Flisikowski K, Eser S, Steiger K, et al. A porcine
811 model of osteosarcoma. *Oncogenesis* 2016; 5: e210. PMID: 26974205. doi:
812 10.1038/oncsis.2016.19.
813 89. Shen Y, Xu K, Yuan Z, Guo J, Zhao H, Zhang X, et al. Efficient generation of P53
814 biallelic knockout Diannan miniature pigs via TALENs and somatic cell nuclear transfer.
815 *J Transl Med* 2017; 15(1): 224. PMID: 29100547. doi: 10.1186/s12967-017-1327-0.
816 90. Luo Y, Kofod-Olsen E, Christensen R, Sorensen CB, Bolund L. Targeted genome editing
817 by recombinant adeno-associated virus (rAAV) vectors for generating genetically
818 modified pigs. *J Gen Genom* 2012; 39(6): 269-74. PMID: 22749014. doi:
819 10.1016/j.jgg.2012.05.004.
820 91. Schachtschneider K, Schwind R, Darfour-Oduro K, De A, Rund L, Singh K, et al. A
821 validated, transitional and translational porcine model of hepatocellular carcinoma.
822 *Oncotarget* 2017: Epub ahead of print, 2017 Jun 29. PMID: 28733541. doi:
823 10.18632/oncotarget.18872.
824 92. Callesen MM, Arnadottir SS, Lyskjaer I, Orntoft MW, Hoyer S, Dagnaes-Hansen F, et al.
825 A genetically inducible porcine model of intestinal cancer. *Mol Oncol* 2017; 11(11):
826 1616-29. PMID: 28881081. doi: 10.1002/1878-0261.12136.
827 93. Remmers N, Cox J, Grandgenett P, Grunkemeyer J, Rund L, Schook L, et al.
828 Development of a Porcine Model of Pancreatic Cancer [poster]. Annual Meeting of the

829 American Association of Cancer Research; Washington, D.C. April 1-5, 2017.
830 http://cancerres.aacrjournals.org/content/77/13_Supplement/813.short
831 94. Smit VT, Boot AJ, Smits AM, Fleuren GJ, Cornelisse CJ, Bos JL. KRAS codon 12
832 mutations occur very frequently in pancreatic adenocarcinomas. *Nucleic Acids Res* 1988;
833 16(16): 7773-82. PMID: 3047672. doi:
834 95. Jones S, Zhang X, Parsons DW, Lin JC, Leary RJ, Angenendt P, et al. Core signaling
835 pathways in human pancreatic cancers revealed by global genomic analyses. *Science*
836 2008; 321(5897): 1801-6. PMID: 18772397. doi: 10.1126/science.1164368.
837 96. Muller PA, Vousden KH. p53 mutations in cancer. *Nat Cell Biol* 2013; 15(1): 2-8. PMID:
838 23263379. doi: 10.1038/ncb2641.
839 97. Olivier M, Hollstein M, Hainaut P. TP53 mutations in human cancers: origins,
840 consequences, and clinical use. *Cold Spring Harbor Perspectives in Biology* 2010; 2(1).
841 PMID: 20182602. doi: 10.1101/cshperspect.a001008.
842 98. Blackford A, Serrano OK, Wolfgang CL, Parmigiani G, Jones S, Zhang X, et al. SMAD4
843 gene mutations are associated with poor prognosis in pancreatic cancer. *Clin Cancer Res*
844 2009; 15(14): 4674-9. PMID: 19584151. doi: 10.1158/1078-0432.CCR-09-0227.
845 99. Caldas C, Hahn SA, da Costa LT, Redston MS, Schutte M, Seymour AB, et al. Frequent
846 somatic mutations and homozygous deletions of the p16 (MTS1) gene in pancreatic
847 adenocarcinoma. *Nat Genet* 1994; 8(1): 27-32. PMID: 7726912. doi: 10.1038/ng0994-27.
848 100. Bardeesy N, Cheng KH, Berger JH, Chu GC, Pahler J, Olson P, et al. Smad4 is
849 dispensable for normal pancreas development yet critical in progression and tumor
850 biology of pancreas cancer. *Genes Dev* 2006; 20(22): 3130-46. PMID: 17114584. doi:
851 10.1101/gad.1478706.

852 101. Bardeesy N, Aguirre AJ, Chu GC, Cheng KH, Lopez LV, Hezel AF, et al. Both
853 p16(Ink4a) and the p19(Arf)-p53 pathway constrain progression of pancreatic
854 adenocarcinoma in the mouse. *Proc Natl Acad Sci U S A* 2006; 103(15): 5947-52. PMID:
855 16585505. doi: 10.1073/pnas.0601273103.
856 102. Wang K, Jin Q, Ruan D, Yang Y, Liu Q, Wu H, et al. Cre-dependent Cas9-expressing
857 pigs enable efficient in vivo genome editing. *Genome Res* 2017; 27(12): 2061-71. PMID:
858 29146772. doi: 10.1101/gr.222521.117.
859 103. Ryu J, Prather RS, Lee K. Use of gene-editing technology to introduce targeted
860 modifications in pigs. *J Anim Sci Biotechnol* 2018; 9: 5. PMID: 29423214. doi:
861 10.1186/s40104-017-0228-7.
862
863

Acknowledgements

This study is the result of work supported in part with resources and the use of facilities at the Omaha VA Medical Center (Nebraska-Western Iowa Health Care System). Portions of this study were presented at the 108th Annual Meeting of the American Association for Cancer Research (AACR) in Washington, D.C., April 1-5, 2017. The authors would like to acknowledge the technical assistance of Gerri Siford, Chris Hansen, Kelly O'Connell, and Tom Caffrey. The authors also would like to thank Dr. Lawrence B. Schook and Dr. Laurie A. Rund at the University of Illinois for the gift of their plasmid that contained the *KRAS*^{G12D} mutation, along with comments, insights and suggestions for its use in this project. Datasets from this manuscript will be freely shared upon request to the senior author (MAC).

877 # Author Contributions

Contributor Role	Description	Author
Conceptualization	Ideas; formulation or evolution of overarching research goals and aims.	MAC
Data Curation	Management activities to annotate (produce metadata), scrub data and maintain research data (including software code, where it is necessary for interpreting the data itself) for initial use and later reuse.	NR, JLC, JAG, SA
Formal Analysis	Application of statistical, mathematical, computational, or other formal techniques to analyze or synthesize study data.	NR, MAC, SA
Funding Acquisition	Acquisition of the financial support for the project leading to this publication.	MAC
Investigation	Conducting a research and investigation process, specifically performing the experiments, or data/evidence collection.	NR, JLC, JAG, SA, MAC
Methodology	Development or design of methodology; creation of models.	NR, MAH, MAC
Project Administration	Management and coordination responsibility for the research activity planning and execution.	MAC
Resources	Provision of study materials, reagents, materials, patients, laboratory samples, animals, instrumentation, computing resources, or other analysis tools.	MAH, SA, MAC
Software	Programming, software development; designing computer programs; implementation of the computer code and supporting algorithms; testing of existing code components.	na
Supervision	Oversight and leadership responsibility for the research activity planning and execution, including mentorship external to the core team.	MAH, MAC
Validation	Verification, whether as a part of the activity or separate, of the overall replication/reproducibility of results/experiments and other research outputs.	NR, JLC, JAG, SA
Visualization	Preparation, creation and/or presentation of the published work, specifically visualization/data presentation.	NR, MAC
Draft Preparation	Creation and/or presentation of the published work, specifically writing the initial draft (including substantive translation).	NR, MAC
Review & Editing	Preparation, creation and/or presentation of the published work by those from the original research group, specifically critical review, commentary or revision – including pre- or post-publication stages.	NR, JLC, JAG, SA, MAH, MAC

878

879 na = not applicable.

880 **Table 1. Tumorigenic cell lines and their expression products.**
881

Cell line	AcGFP1 protein	$KRAS^{G12D}$ protein	$p53^{R167H}$ protein	SMAD4 shRNA	$p16^{Ink4A}$ shRNA
PGKP	+	+	+		
PGKPS	+	+	+	+	
PGKPSC*	+	+	+	+	+

882
883 All cell lines based on primary porcine pancreatic ductal epithelial cells. *Abbreviation key: **P** =
884 pancreatic ductal epithelium; **G** = GFP; **K** = KRAS; **P** = p53; **S** = SMAD4; **C** =
885 $p16^{Ink4A}$/CDKN2A.
886

887 **Figure Legends**

888

889 **Fig. 1. Isolation and transduction of primary porcine pancreatic ductal epithelial cells.** (A)
890 Phase image of cells isolated from porcine pancreatic duct, showing epithelial-like morphology
891 (bar = 1,000 µm). (B) Immunofluorescent staining for cytokeratin 19 in the cultured primary
892 cells (bar = 200 µm). (C) Immunoblot for the p53 mutant in nine different cells lines transduced
893 with the GKP virus (PGKP cells). Pancreas = wild type pancreatic ductal epithelial cells.
894 Representative blot of three separate experiments. (D-E) qPCR of KRAS and p53 mutants in the
895 nine PKGP cell lines. Each bar represents mean of three separate experiments. *$p<0.05$, **
896 $p<0.03$, ***$p<0.01$ (unpaired t-test, compared to wild type).

897

898 **Fig. 2. Effect of SMAD4 and $p16^{Ink4A}$ knockdown on transformation in the PGKP cell line.**
899 (A) Soft agar assay and (B) migration assay in the nine GKP-transduced cell lines. Pancreas =
900 wild type pancreatic ductal epithelial cells. Each bar represents mean of three separate
901 experiments. (C) RT-PCR of SMAD4 and $p16^{Ink4A}$/CDKN2A mRNA in cell lines expressing
902 targeted or scramble shRNA. Representative blot of three separate experiments. (D) Soft agar
903 assay and (E) migration assay of selected cell lines (PGKP, PGKPS, and PGKPSC), showing the
904 *in vitro* effect of additional knockdown of SMAD4 ± $p16^{Ink4A}$ on the transformation of GKP-
905 transduced pancreatic ductal epithelial cells.

906

907 **Fig. 3. *In vitro* transformation assays comparing the PGKP, PGKPS, and PGKPSC cell**
908 **lines**. (A) Cell culture population doubling time (count-based assay). Pancreas = wild type
909 pancreatic ductal epithelial cells. (B) Proliferation rate (metabolic dye-based assay), represented

910 as fold change, normalized to wild type cells. (C) Invasion (Matrigel®-based assay). Each bar or
911 data point represents mean of three separate experiments.
912
913 **Fig. 4. *In vivo* tumorigenesis assays comparing the PGKP, PGKPS, and PGKPSC cell lines**.
914 (A) Sample of a resected tumor from subcutaneous injection in nude mice; note size and
915 vascularity. (B) Tumor growth curve from the subcutaneous injection in nude mice. Each data
916 point represents mean of 10 mice. (C) Metastasis after orthotopic implantation in nude mice
917
918 **Fig. 5. Tumor immunohistochemistry from subcutaneous nude mouse assay.** Representative
919 images of primary tumors derived from the PGKP, PGKPS, and PGKPSC cell lines stained with
920 an array of epithelial markers, including E-cadherin (Ecad; B, G, L), Epithelial Cell Adhesion
921 Molecule (EpCAM; C, H, M), Pan-Cytokeratin (PanCK; D, I, N), and Cytokeratin-19 (CK19; E,
922 J, O); and also stained with mesenchymal markers, including α-Smooth Muscle Actin (SMA; P,
923 S, V), Vimentin (Vim; Q, T, W), and Type I Collagen (Col I; R, U, X). Bar = 200 μm.
924

925 # Supporting Information

926

927 **Fig. S1**. pIRES2-AcGFP1 Vector Information

928 **Fig. S2**. Studies with the NSRRC KRAS/p53 Oncopig

929 **Fig. S3**. KRAS/p53 immunohistochemistry of subcutaneous murine tumors

930 **Protocol S1.** Isolation of Epithelial Cells from Porcine Pancreas

931 **Protocol S2**. Porcine methodology

932 **Table S1**. Responses to the ARRIVE recommendations

933 **Table S2**. Responses to the NIH Preclinical Research Guidelines

934 **Table S3**. Primers and other short sequences

935 **Table S4**. Antibody information

936 **Table S5**. Oncopig descriptive data

937 **Table S6**. Oncopig serum laboratory testing

938

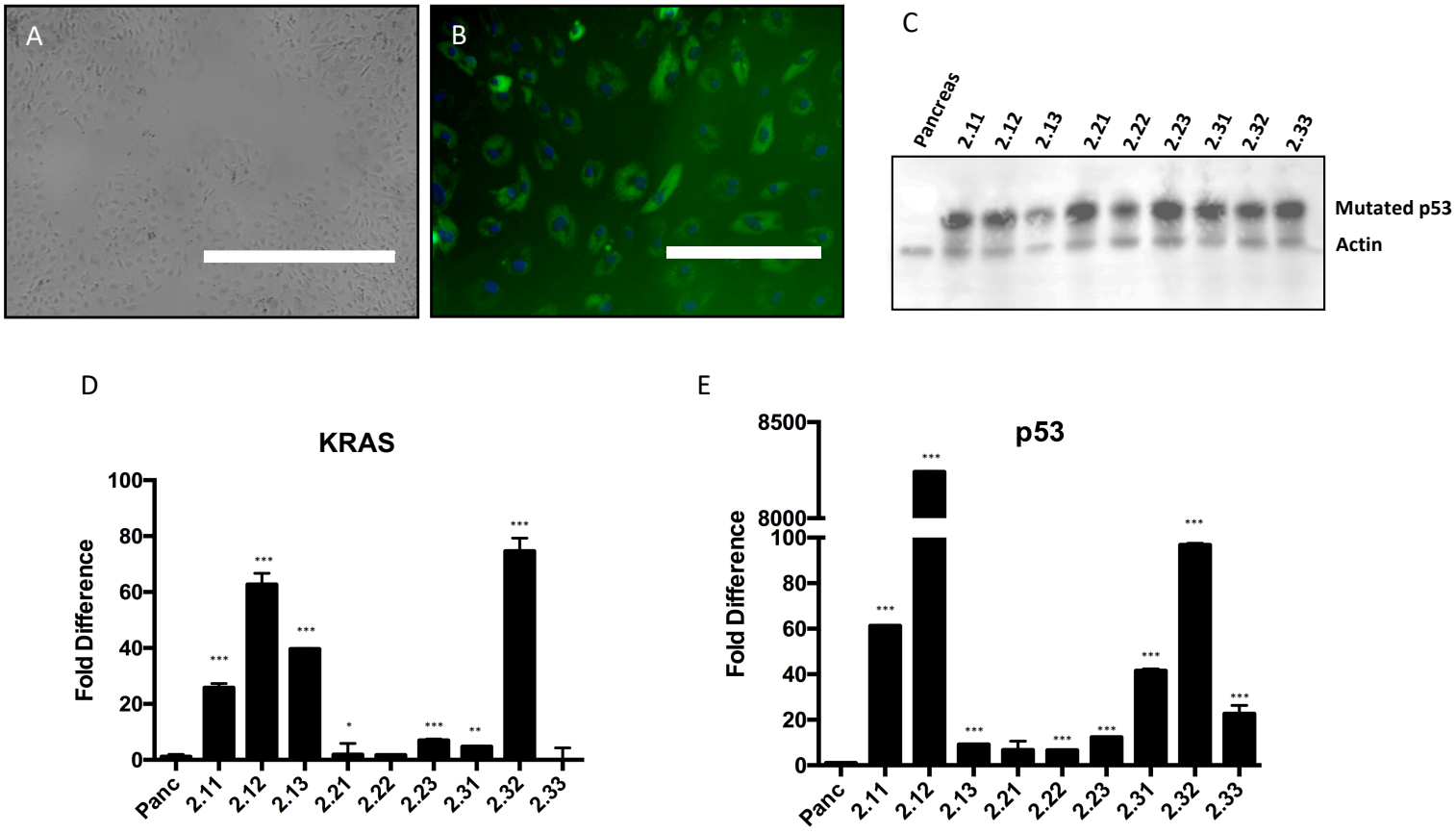
A
B
C
Pancreas
2.11
2.12
2.13
2.21
2.22
2.23
2.31
2.32
2.33
Mutated p53
Actin
D
KRAS
Fold Difference
100
80
60
40
20
0
Panc
2.11
2.12
2.13
2.21
2.22
2.23
2.31
2.32
2.33
E
p53
Fold Difference
8500
8000
100
80
60
40
20
0
Panc
2.11
2.12
2.13
2.21
2.22
2.23
2.31
2.32
2.33

Figure 1

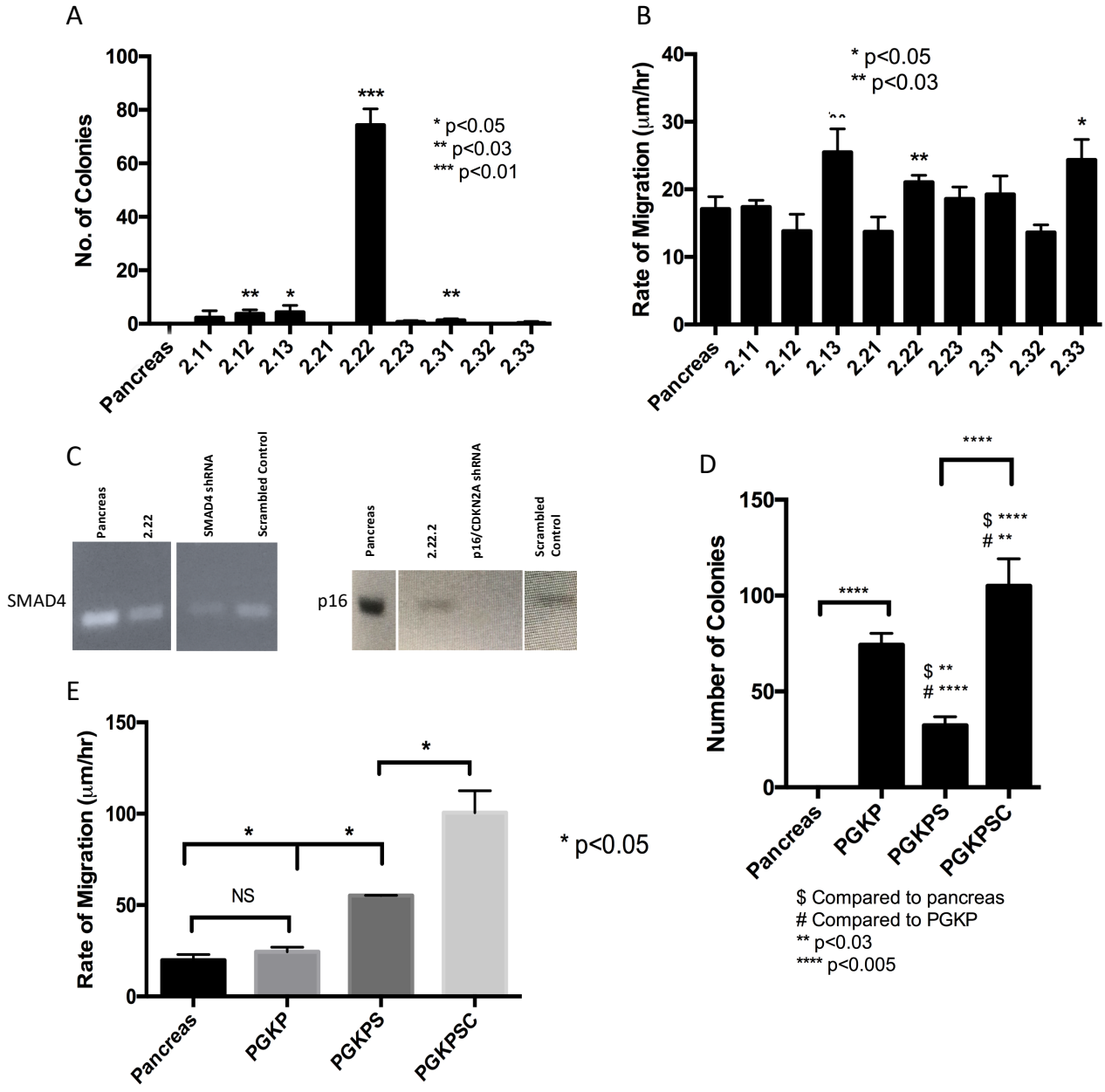
A
No. of Colonies
100
80
60
40
20
0
***
**
*
**
* p<0.05
** p<0.03
*** p<0.01
Pancreas
2.11
2.12
2.13
2.21
2.22
2.23
2.31
2.32
2.33
B
Rate of Migration (μm/hr)
40
30
20
10
0
* p<0.05
** p<0.03
**
**
*
Pancreas
2.11
2.12
2.13
2.21
2.22
2.23
2.31
2.32
2.33
C
Pancreas
2.22
SMAD4 shRNA
Scrambled Control
SMAD4
Pancreas
2.22.2
p16/CDKN2A shRNA
Scrambled Control
p16
D
Number of Colonies
150
100
50
0
****
****
$ ****
# **
$ **
# ****
Pancreas
PGKP
PGKPS
PGKPSC
$ Compared to pancreas
# Compared to PGKP
** p<0.03
**** p<0.005
E
Rate of Migration (μm/hr)
150
100
50
0
*
*
*
NS
* p<0.05
Pancreas
PGKP
PGKPS
PGKPSC

Figure 2

A

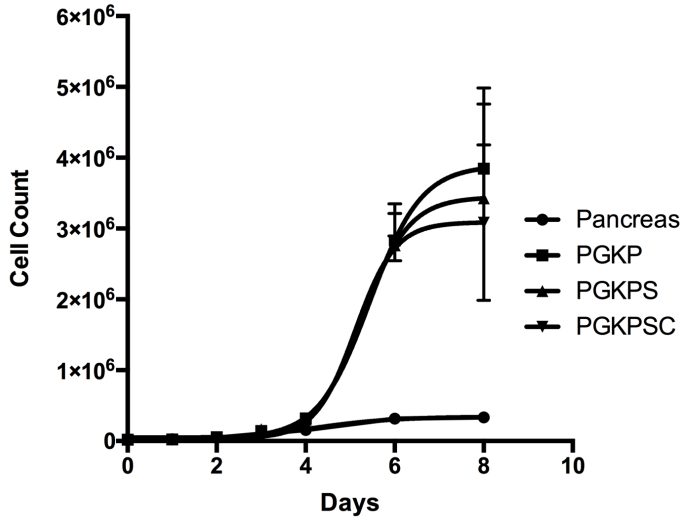
6×10^6
5×10^6
4×10^6
3×10^6
2×10^6
1×10^6
0
Cell Count
0
2
4
6
8
10
Days
Pancreas
PGKP
PGKPS
PGKPSC

B

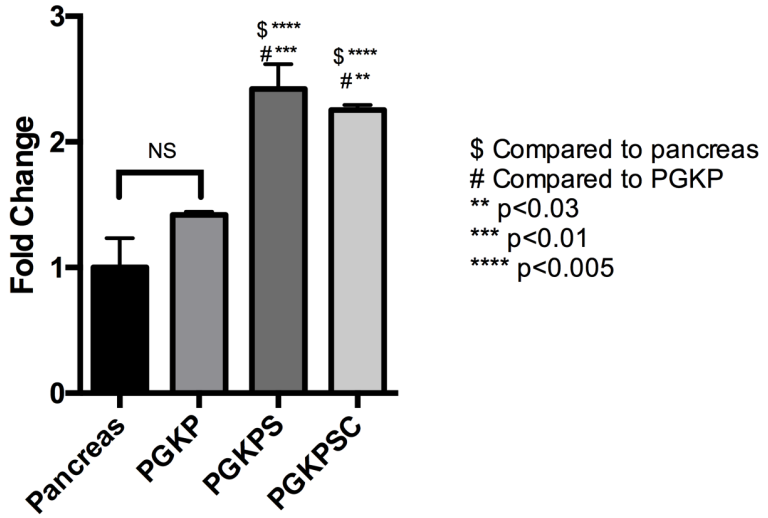
3
2
1
0
Fold Change
NS
$ ****
#***
$ ****
#**
Pancreas
PGKP
PGKPS
PGKPSC
$ Compared to pancreas
# Compared to PGKP
** p<0.03
*** p<0.01
**** p<0.005

C

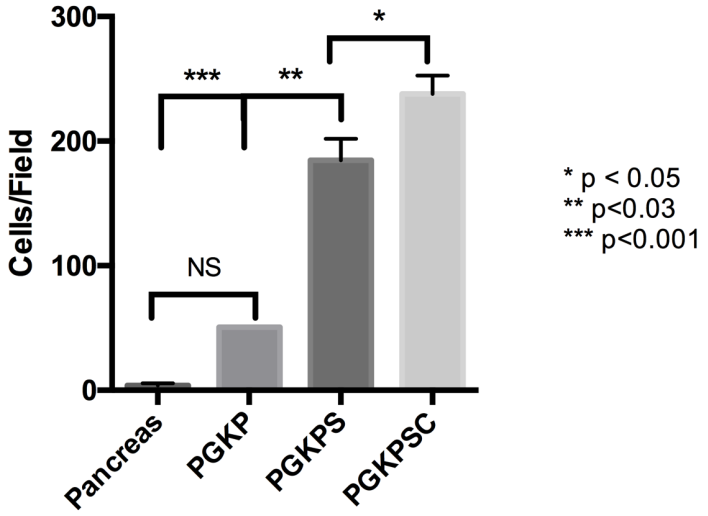
300
200
100
0
Cells/Field
***
**
*
NS
Pancreas
PGKP
PGKPS
PGKPSC
* p < 0.05
** p<0.03
*** p<0.001

Figure 3

A
CM 1 2 3 4 5

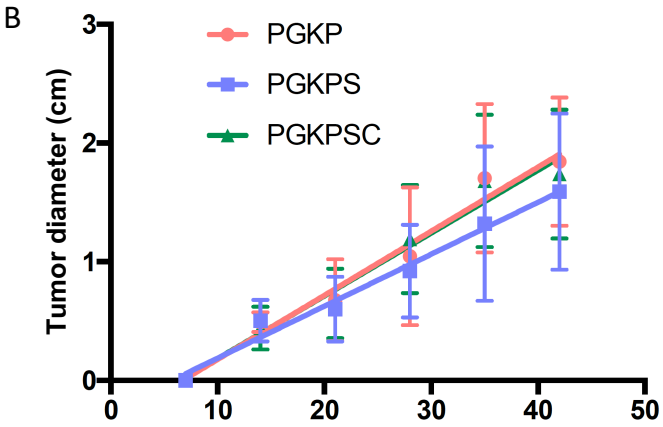
B
PGKP
PGKPS
PGKPSC
Tumor diameter (cm)
0
1
2
3
0
10
20
30
40
50

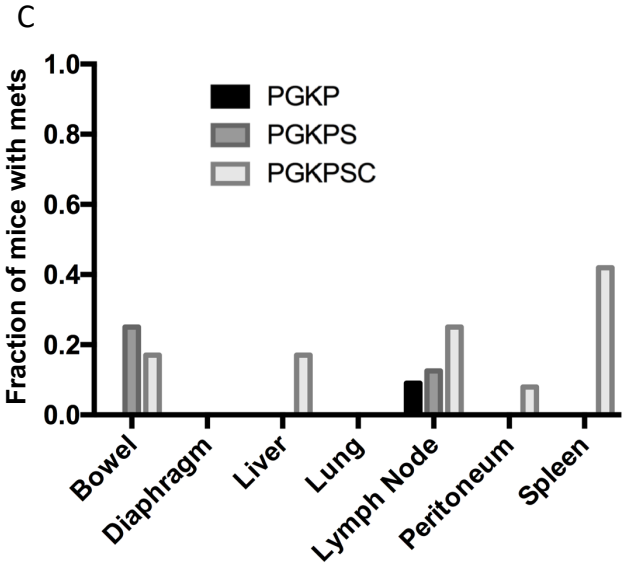
C
PGKP
PGKPS
PGKPSC
Fraction of mice with mets
0.0
0.2
0.4
0.6
0.8
1.0
Bowel
Diaphragm
Liver
Lung
Lymph Node
Peritoneum
Spleen

Figure 4

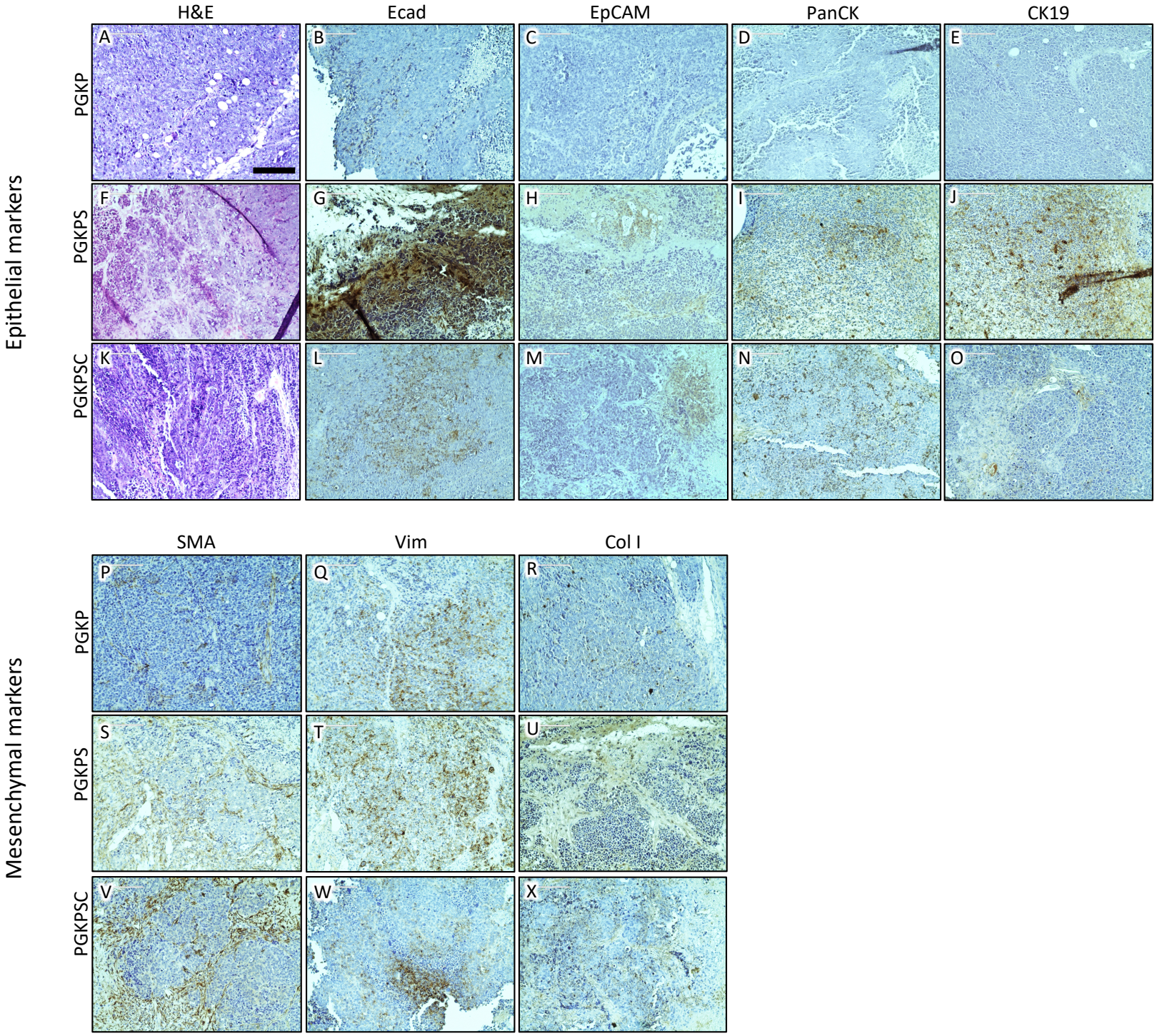
H&E
Ecad
EpCAM
PanCK
CK19
Epithelial markers
PGKP
PGKPS
PGKPSC
A
B
C
D
E
F
G
H
I
J
K
L
M
N
O
SMA
Vim
Col I
Mesenchymal markers
P
Q
R
S
T
U
V
W
X

Figure 5